Supplementary Information: PASCAL: the Perovskite Automated Spin Coat Assembly Line Accelerates Composition Screening in Triple-Halide Perovskite Alloys

Deniz N. Cakan[‡], Rishi E. Kumar[‡], Eric Oberholtz, Moses Kodur, Jack R. Palmer, Apoorva Gupta, Ken Kaushal, Hendrik M. Vossler, and David P. Fenning

Contents

List of Tables

List of Figures

[0]*Department of Nanoengineering, University of California San Diego, La Jolla, CA, 92093, USA; E-mail: dfenning@ucsd.edu*
[0]‡ These authors contributed equally to this work as above using the symbols: ‡

Table S1 Average feature values of clusters.

Cluster labels	PL peak energy (eV)	PL intensity (a.u.)	Photo: PL intensity change (I/I0)	Thermal: PL intensity change (I/I0)	Photo: PL peak shift (I-I0, meV)	Thermal: PL peak shift (I-I0, meV)
Brightest PL	1.63	5.5	1.05	0.27	-10	28.5
PL blueshift & brighten	1.62	1.22	1.57	0.31	-2.7	17.3
PL blueshift	1.66	1.15	0.99	0.17	0.4	29.4
Most stable PL energy	1.66	0.62	0.71	0.16	0.7	-0.4

Table S2 Average PL peak shift after thermal and photo-exposure for a $MA_{0.035}FA_{0.78}Cs_{0.185}Pb(I_{0.863}Br_{0.132}Cl_{0.005})_3$ composition thin film.

Test	PL peak shift (meV)
Photo	-0.53 ± 0.09
Thermal	-0.66 ± 0.12

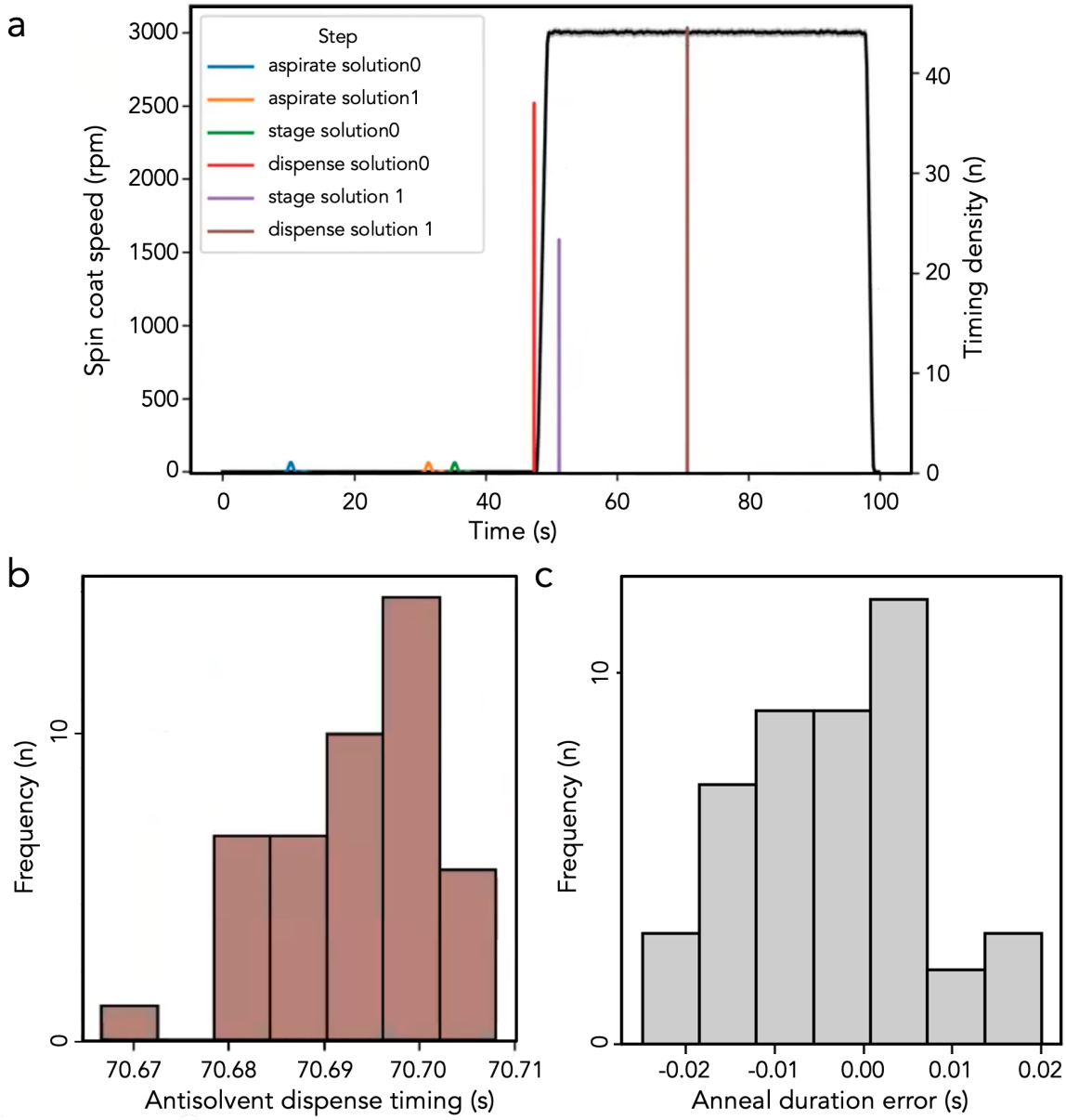

Figure S1 Example timing distribution of a typical 45-sample fabrication with an antisolvent process. a) Example RPM record and timing. RPM trace in black, and antisolvent timing density in brown. b) Histogram zoom into timing density for antisolvent drop timing. c) Histogram of anneal duration error (actual - target).

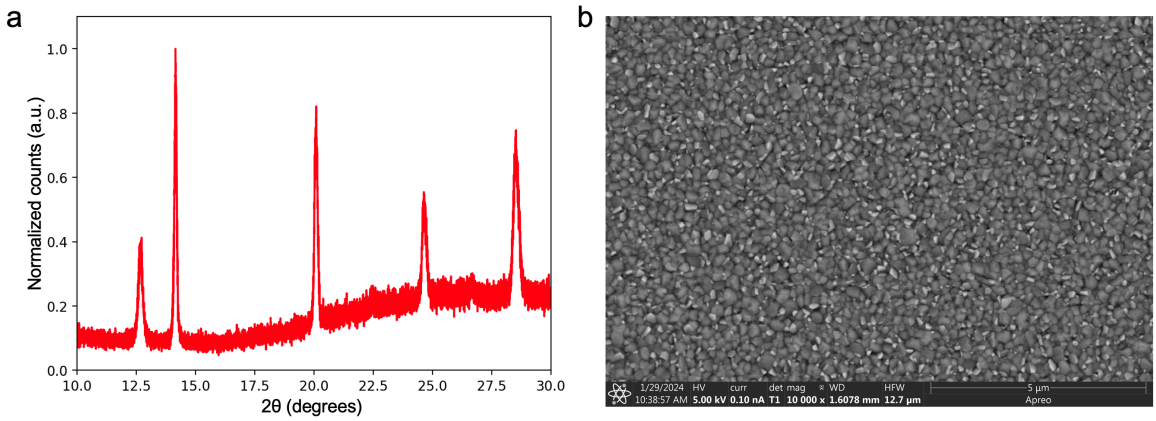

Figure S2 a) XRD and b) SEM of a $Cs_{0.22}FA_{0.78}Pb(I_{0.85}Br_{0.15})_3$ composition film on glass. XRD measured in parallel-beam mode at ω=10° .

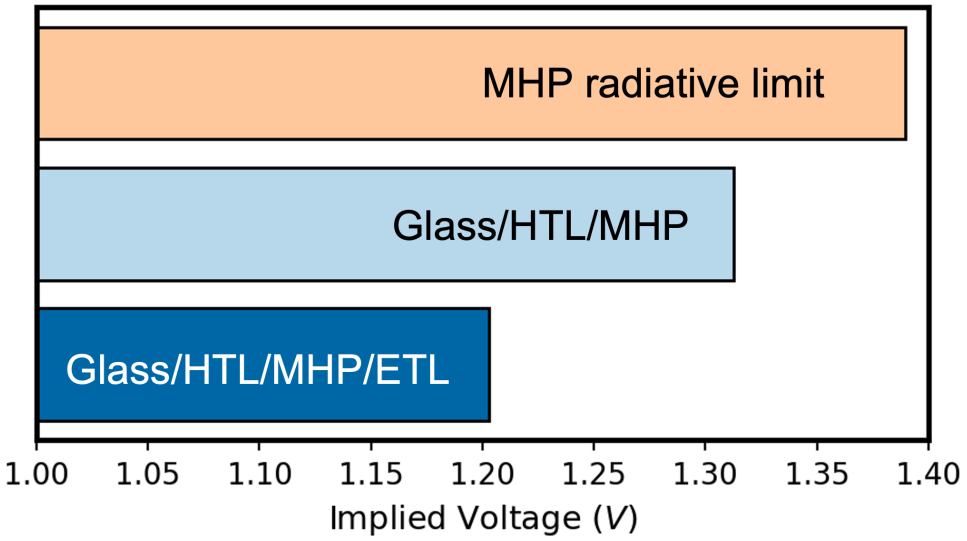

Figure S3 iVoc on subcell architectures calculated from PLQY and the 1.67eV MHP detailed balance limit.

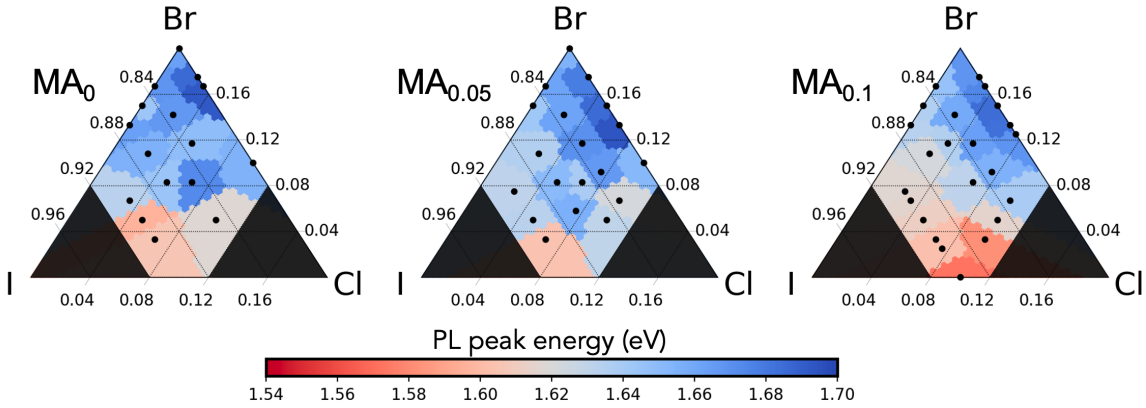

Figure S4 PL peak energy for $MA_xFA_{0.78}Cs_{0.22-x}Pb(I_{0.8-y-z}Br_yCl_z)_3$ films. Corresponding MA content is listed above each ternary, with shared color bar below.

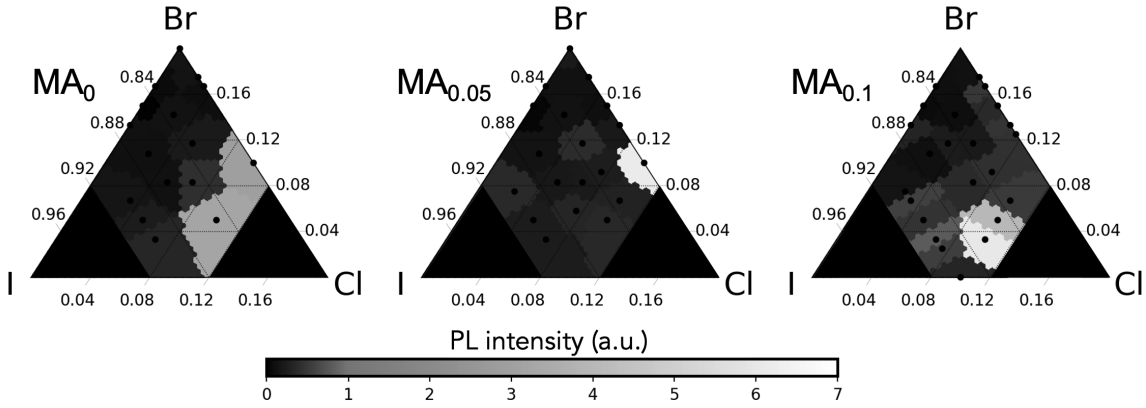

Figure S5 PL intensity of $MA_xFA_{0.78}Cs_{0.22-x}Pb(I_{0.8-y-z}Br_yCl_z)_3$ films, MA content above ternary, with color bar below.

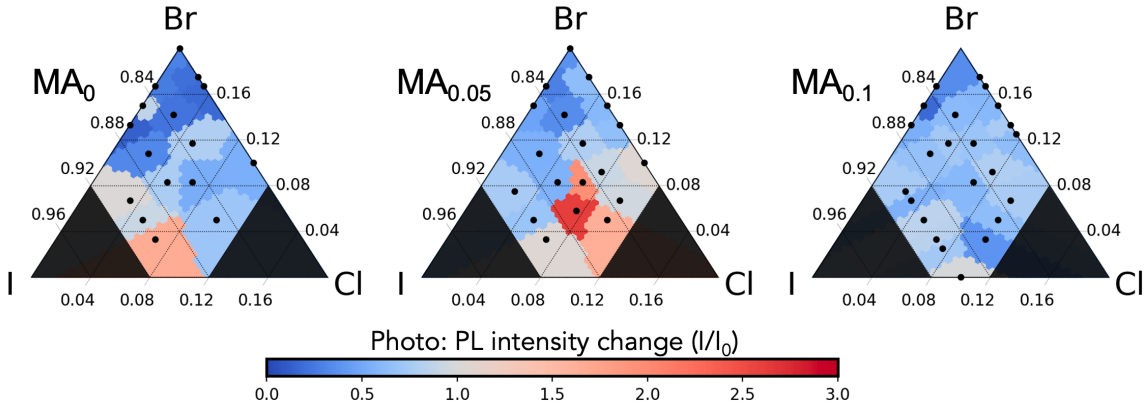

Figure S6 Change in PL intensity after photoexposure of $MA_xFA_{0.78}Cs_{0.22-x}Pb(I_{0.8-y-z}Br_yCl_z)_3$ films, MA content above ternary, with color bar below.

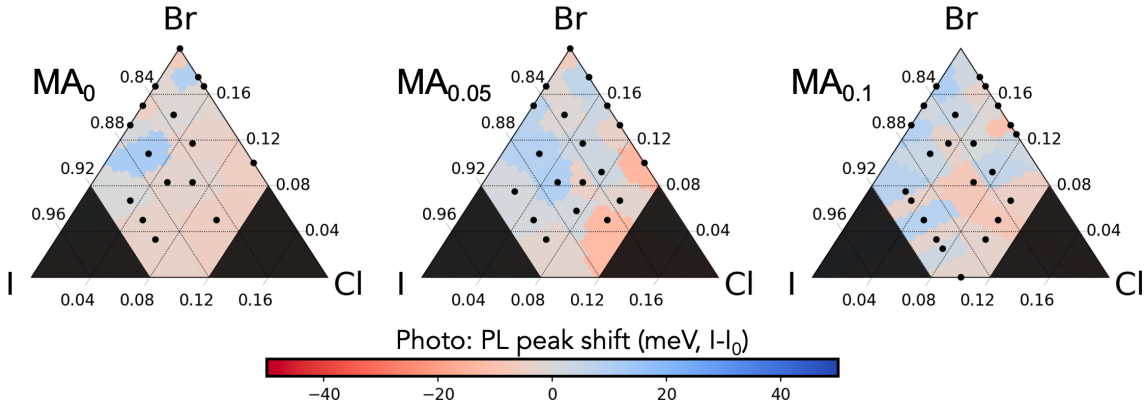

Figure S7 PL peak shift after photoexposure for $MA_xFA_{0.78}Cs_{0.22-x}Pb(I_{0.8-y-z}Br_yCl_z)_3$ films, MA content above ternary, with color bar below.

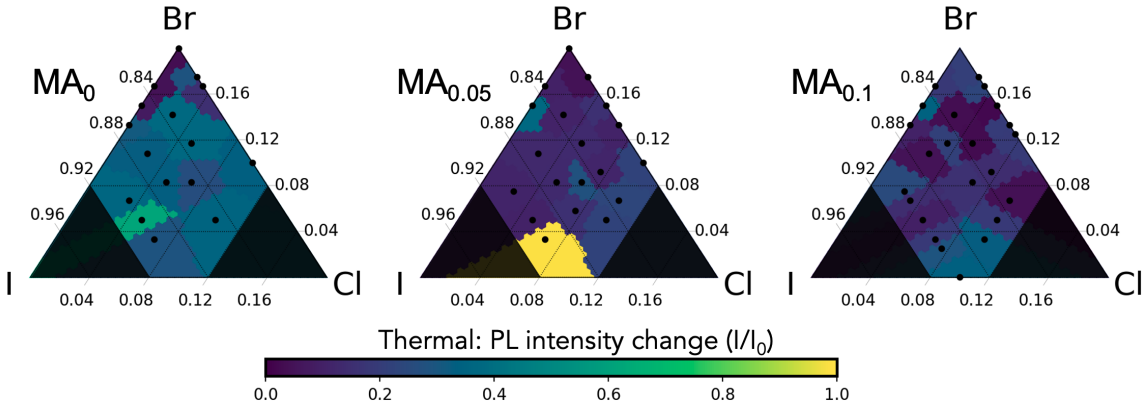

Figure S8 PL intensity change after thermal degradation of $MA_xFA_{0.78}Cs_{0.22-x}Pb(I_{0.8-y-z}Br_yCl_z)_3$ films, MA content above ternary, with color bar below.

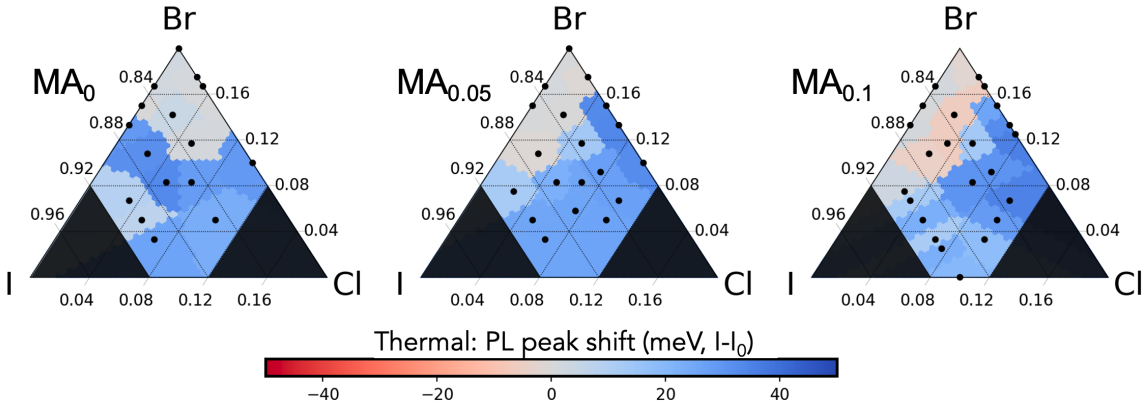

Figure S9 PL peak shift after thermal testing of $MA_xFA_{0.78}Cs_{0.22-x}Pb(I_{0.8-y-z}Br_yCl_z)_3$ films, MA content above ternary, with color bar below.

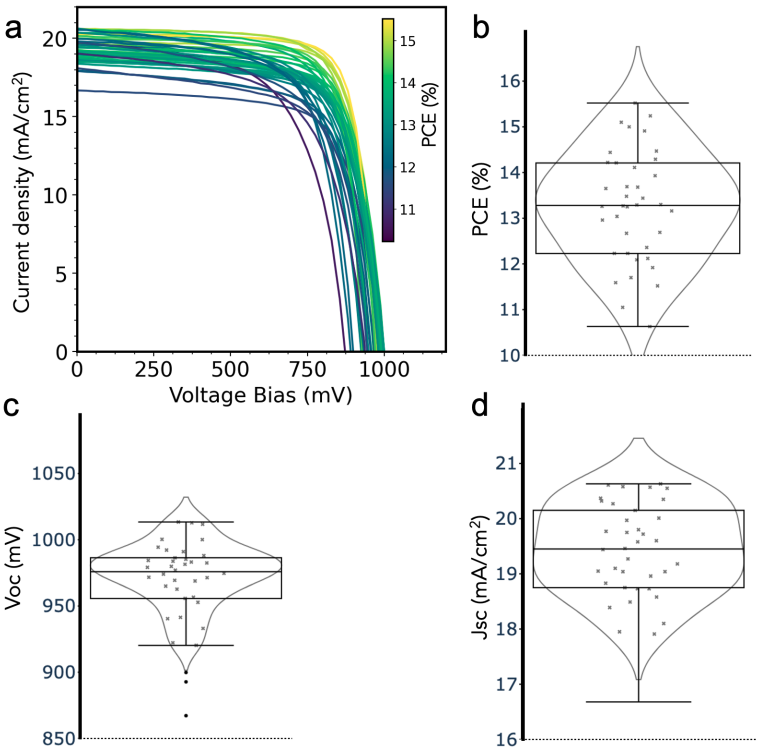

Figure S10 Reverse scan JV curves of prototype device of a $MA_{0.035}FA_{0.78}Cs_{0.185}Pb(I_{0.863}Br_{0.132}Cl_{0.005})_3$ composition. Box plots of device b) PCE, c) Voc, d) Jsc metrics.